Slowly migrating fracture swarms in an actively serpentinizing borehole

John M. Aiken[1,2], Fabian Barras[1], François Renard[1,3], Greg Hirth[4], Peter B. Kelemen[5], Robert A. Sohn[6]

[1]Njord Centre, Departments of Geosciences and Physics, University of Oslo, PO BOX 1048, Blindern, 0316 Oslo, Norway
[2]Expert Analytics, Oslo, Norway
[3]ISTerre, Univ. Grenoble Alpes, Grenoble INP, Univ. Savoie Mont Blanc, CNRS, IRD, Univ. Gustave Eiffel, 1381 rue de la Piscine, 38000 Grenoble, France
[4]Department of Earth, Environmental, and Planetary Sciences, Brown University, Providence, RI, USA
[5]Lamont-Doherty Earth Observatory, Columbia University, Palisades, NY, USA
[6]Department of Geology and Geophysics, Woods Hole Oceanographic Institution, 266 Woods Hole Rd., Woods Hole, MA 02543, USA

Key Points:

- Hydrophones have detected slow propagating fracture swarms in a borehole in Oman peridotites.
- Fracture swarms occur due the combination of chemical weakening and pore pressure changes due to rain.
- These field observations show evidence for fracturing occurring in a low-temperature, active serpentinizing environment.

Corresponding author: John M. Aiken, `johnm.aiken@gmail.com`

Abstract

Peridotite rocks are primary targets for engineered geological carbon sequestration efforts because they accomodate transfer carbon from aqueous fluids to rock during alteration reactions. Sequestration efforts must necessarily open fractures in the rocks surrounding a pumped borehole, but the current understanding of fracture growth during serpentinization of peridotite is limited to theoretical models and laboratory experiments on small samples. We deployed hydrophone arrays in peridotite boreholes established by the Oman Drilling Program and detected downward migrating earthquake swarms that represent the first field observations of active fracture growth in a serpentinizing rock. More than two years after the boreholes were established, we detected four fracture swarms during an interval of elevated pore pressure following large rain events. All of the swarms occurred within a partially-confined section of the local aquifer, beginning at a depth of ∼170 m and migrating to the bottom of the 400 m-deep hole at average rates of ∼6-20 cm.s^{-1}. Pore fluid processes can explain both triggering of the fracture swarms and their slow migration rates, which are characteristic of slow earthquakes, and water-rock reactions likely play a role in maintaining near-critical stresses at the crack tips as fractures grow away from the borehole. Our results indicate that fractures propagating away from actively serpentinizing boreholes maintain near-critical crack tip stresses such that relatively small increases in fluid pressure can trigger tensile fracturing episodes, and that pore fluid processes can limit the propagation speed of these tensile fractures in much the same way as they do for shear fractures.

Plain Language Summary

Scientists are exploring ways to store carbon dioxide underground by pumping carbonated water into deep holes drilled in special rocks called peridotites. These rocks can react with the water and carbon dioxide to form new minerals, which locks away the carbon safely. This study monitored two boreholes in Oman and found that, even years after drilling, new fractures formed in the rock during times of high water pressure and chemical changes. The fractures grew slowly, likely because water was moving into the cracks as they formed. These findings show that chemical reactions between water, carbon dioxide, and rock can help create new pathways for fluids, which is important for improving carbon storage in the future.

1 Introduction

Pumping carbonated water into boreholes drilled into mafic rocks, such as basalts or peridotites, is an emergent technology of engineered geological carbon sequestration (Gislason and Oelkers 2014). In peridotites, the water-rock reactions transfer CO_2 from the water to the rock via mineral carbonation and serpentinization, and the effectiveness of this approach depends on the ability to stimulate fracture growth to open pore space and expose fluids to fresh rock. Peridotite rocks have low bulk permeability but contain complex multidirectional fracture networks that support fluid flow and ongoing alteration (Iyer et al. 2008; Kelemen, James A. Leong, et al. 2021; Aiken et al. 2024). The serpentinization and carbonation water-rock reactions increase the solid volume of the rock and exert a force of crystallization, and it has been hypothesized that the resulting stress perturbation facilitates the opening of new fractures, which in turn sustains ongoing alteration (Kelemen and Jürg Matter 2008; Jamtveit, Putnis, and Malthe-Sørenssen 2009; Renard 2021). This *reaction-driven fracturing* hypothesis predicts that crack tip stresses in active alteration zones will continually increase and reach critical levels for failure, which, if true, should facilitate the opening of new fracture surface area for carbon sequestration efforts.

The Multi-Borehole Observatory (MBO) of the Oman Drilling Program (OmanDP) is located in Wadi Lawayni, a dry wash that cuts through mantle rocks of the Samail ophiolite in Oman (Figure 1). The MBO established four boreholes, providing a unique opportunity to study near-surface peridotite alteration and the chemosynthetic biosphere that feeds on the reaction byproducts ((Kelemen, James A. Leong, et al. 2021; Templeton et al. 2021; Hatakeyama et al. 2021; Callegari et al. 2022; Sohn and J.M. Matter 2023)), and, ultimately, to begin to test the reaction-driven fracturing hypothesis. Here we used downhole hydrophone arrays to monitor fracturing on the walls of two boreholes, spaced 100 m apart, for nine months.

The introduction of a circular opening into rock generates tangential stress concentrations around the borehole walls, and if the stress exceeds the rock strength the wall will fracture and deform (Jaeger, N. G. Cook, and Zimmerman 2009). Both compressional and tensile failure can occur, and the nature of the deformation depends on the magnitudes of the local principal stresses, the pore fluid pressure in the surrounding rock matrix, and the tensile strength of the wall rocks (e.g. (Zoback et al. 1985; Zheng, Kemeny, and N. G. W. Cook 1989)). In a peridotite borehole, however, it is also necessary to consider the effect of alteration. A variety of theoretical models and laboratory experiments have been developed and conducted to study reaction-driven fracture propagation during peridotite alteration (e.g., (Kelemen, James A. Leong, et al. 2021; Kelemen and Jürg Matter 2008; Jamtveit, Putnis, and Malthe-Sørenssen 2009; Kelemen, Juerg Matter, et al. 2011)), but none have been conducted in the context of a drilling-induced stress field; critically, there are no field observations of active fracture growth in peridotite boreholes. It is typically assumed that borehole deformation occurring from drilling and coring happens in the first hours to days following the creation of a borehole (Moore et al. 2011). After this, the stresses around the borehole have reorientated to equilibrium and no further borehole damage will occur without either first weakening the rock (e.g., chemically via rock-fluid interactions) and/or decreasing the effective stress (e.g., increasing the pore pressure) (Zoback et al. 1985).

We find that the borehole penetrating a semi-confined portion of the local aquifer experienced fracture swarms more than two years after it was drilled during a period of elevated pore pressure induced by large rain events. The swarms nucleated at approximately the same depth of ∼170 m where we observe an increase in pH and a decrease in oxygen fugacity in the borehole fluids, both indicators of chemical alteration due to rock-fluid interactions. The swarms migrated downward at slow velocities in the range ∼6-20 cm.s^{-1}, demonstrating that dynamic fracture propagation was inhibited. We propose that fluid migration into the newly created pore space at the tip of the propagating fracture can explain the slow rupture speeds, similar to the way they can regulate rupture speeds during slow earthquakes, and that water-rock reactions likely play a key role in maintaining near-critical stress levels as cracks grow over time.

2 Methods

2.1 Site Description

The MBO consists of four, ∼400 m deep boreholes within a ∼100 x 100 m^2 area, three of which were drilled with 15.2 cm diameter (BA1A, BA1C - collapsed, BA1D), and one of which was cored with a 9.6 cm diameter (BA1B) (Kelemen, J.M. Matter, et al. 2020). The lithological structure of the site is constrained by downhole observations and core sample analyses, and overall consists of dunites to a depth of ∼160 m that are underlain by less depleted harzburgites (Kelemen, James A. Leong, et al. 2021). The near-surface zone down to ∼50 m is extensively fractured and contains cross-cutting carbonate and serpentinite veins. Below ∼50 m the degree of fracturing decreases and carbonate alteration is no longer observed. Veins and fractures are sparse below ∼160 m in the harzburgites, with porosities ≤ ∼1% (Katayama et al. 2020). The complex fracturing and alteration history of the rocks is due to a combination of the mid-ocean ridge process during formation and more recent obduction and subaerial weathering. Gases can

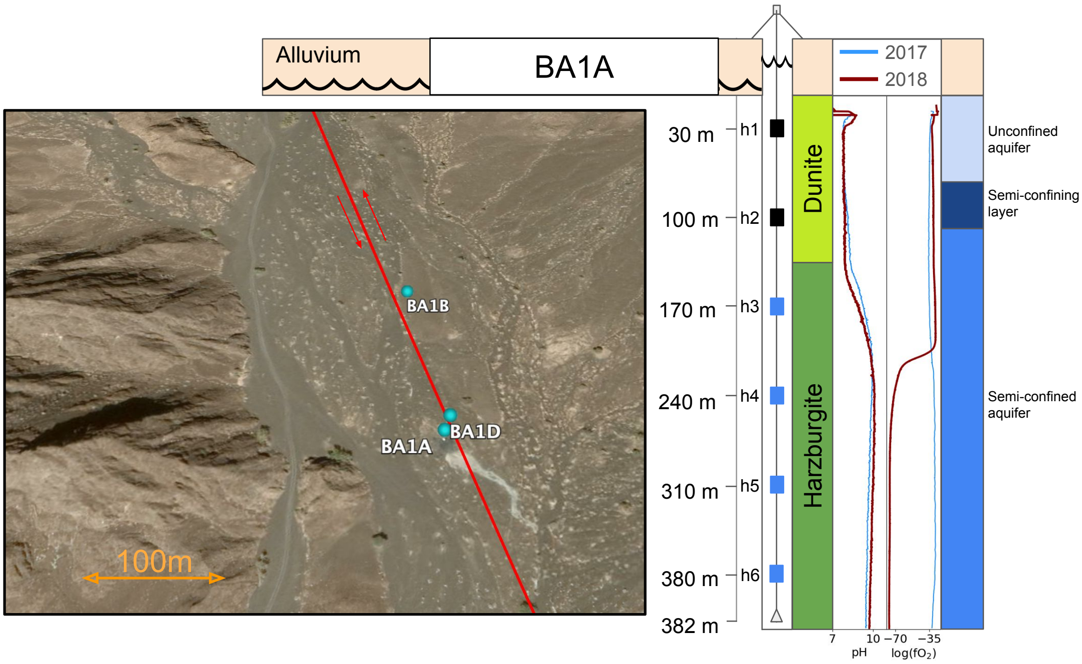

Figure 1. Location of the OmanDP Multi-Borehole Observatory (MBO) in a mantle section of the Samail ophiolite in Wadi Lawayni, Oman. The red line represents a left-lateral fault that transects the MBO (Callegari et al. 2022). Three boreholes (BA1A, BA1B, BA1D) were drilled in a ∼100 x 100 m area (another borehole, BA1C, not shown, collapsed during drilling). Six-element hydrophone arrays were deployed for nine months in boreholes BA1A and BA1B. The fracture swarms described here were detected by the bottom four phones (h3 - h6, colored blue) in borehole BA1A (data from the top two phones, colored black, were corrupted by electrical noise). The increase in pH and drop in oxygen fugacity measured one year after drilling and reported in (Kelemen, James A. Leong, et al. 2021) are reprinted here. The primary lithological (Kelemen, James A. Leong, et al. 2021) and hydrological (Lods et al. 2020) structure of hole BA1A are shown on the right.

be observed bubbling up in alkaline pools on the surface indicating an active subsurface chemistry. This has been confirmed through downhole measurements at the BA site that showed pH increases and oxygen fugacity decreases with depth (Kelemen, James A. Leong, et al. 2021).

The hydrologic structure of the MBO site is heterogeneous but overall consists of a high-permeability near-surface zone underlain by a low-permeability aquifer (Lods et al. 2020). Flow in the near-surface zone ($\leq \sim$50 m depth), corresponding to the zone of intense fracturing in the lithological record, is focused within a network of multi-directional heterogeneities. The aquifer surrounding boreholes BA1A and BA1D is partially confined by a low permeability layer at ∼100-130 m depth, which allows it to be pressurized by external loads. In contrast, pore pressure in the aquifer surrounding borehole BA1B does not respond to barometric or tidal loads, indicating that the aquifer is locally unconfined (Sohn and J.M. Matter 2023). The aquifer response to loading thus changes markedly over the ∼100 m distance between boreholes BA1A and BA1B.

2.2 Rain and Borehole Water Level Data

Using a Rugged TROLL non-vented data logger from In-Situ Inc., we acquired water level at 15 minute intervals in borehole BA1D. The non-vented pressure data were corrected by subtracting contemporaneously measured atmospheric pressure data and converted to relative water level assuming a fluid density of 1000 kg.m^{-3}. We retrieved daily precipitation rates for the MBO catchment from the Copernicus Climate Reanalysis Data Store ((CDS) 2017) using the catchment shape defined by the hydroBASINS data set (Lehner and Grill 2013) (Figure 5). The water levels in borehole BA1D rose rapidly by ∼5 m following two large rain events in April and May 2019 and then slowly decreased until the end of the hydrophone array deployments.

2.3 Televiewer Data

Televiewer data were acquired from depths of 25-400 m in borehole BA1A following its completion in March, 2017. This data was collected as 360 degree Red-Green-Blue images with a pixel resolution of 0.8 mm. Inspection of images reveal the presence of numerous vertical veins that could act as nucleation sites for the vertical propagation of tensile fractures we observed (Figure 6).

2.4 Acoustic Data

We deployed hydrophone arrays, each consisting of six High Tech HTI-96-MIN hydrophones with a 70 m inter-element spacing, in boreholes BA1A and BA1B (Figure 1) from May 2019 to February 2020. The data were sampled at 1 kHz and recorded using a Quanterra Q330S+ data logger with a low-pass (450 Hz) anti-aliasing filter.

We detected downward migrating event swarms in hole BA1A on four days (days 141, 188, 197, and 211) in 2019 (cite swarm figure). We detected individual events within the high-rate swarms by extracting data windows extending from ∼15 minutes before the swarm starts until ∼15 minutes after it ends, high-pass filtering (50 Hz, zero-phase) the extracted records, and squaring the signal amplitude. We generated a preliminary catalog by applying a peak finding algorithm to each processed record and associating detections across the hydrophone array. We generated arrival time estimates by selecting a 0.4 second window centered on the initial detection time, calculating the Akaike Information Criterion (AIC) for each trace (Maeda 1985), and picking arrival times based on the maximum value of the AIC time-derivative.

The arrival time and amplitude of the signals across the vertical hydrophone array exhibit a systematic pattern, with the earliest arrivals having the highest amplitudes and the arrival time difference between the two hydrophones with the earliest arrivals, i.e., the "bounding phones", being between zero and ~40 ms (cite event waveform figure). Signal amplitudes decrease with distance, up or down the array, from the bounding phones and the arrival time difference between all other adjacent hydrophone pairs is a constant value of ~40 ms, corresponding to an apparent phase velocity of ~1750 m.s^{-1}. This phase velocity is too slow for a body wave propagating in the rock, which has compressional velocities of ~5.6 km.s^{-1} and shear velocities of ~2.9 km.s^{-1} (Hatakeyama et al. 2021), but is consistent with a trapped fluid mode originating from a source on the borehole wall and propagating inside the borehole at a velocity faster than the fluid sound speed but slower than the medium shear velocity (Schoenberg et al. 1981). In some cases we observed a smaller precursor arrival with an apparent phase velocity of ~2460 m.s^{-1} that was only detectable on one or both of the bounding hydrophones, indicating that the source also excited a more rapidly decaying higher order mode. There is no evidence for P- or S-waves in the waveforms (Figure 3), consistent with sources located on the borehole wall.

Assuming a trapped fluid mode propagation velocity of 1750 m.s^{-1} and given the 70 m vertical offset between the hydrophones, the source depth of an event can be estimated based on the arrival time difference between the bounding phones. If the phase arrives at the upper bounding hydrophone with depth z_i at time t_i, and arrives at the lower bounding hydrophone at time t_j, then given the 70 m offset of the hydrophones the source depth, z, is given by (Figure 3):

$$z = z_i + 35 - 0.5 \times dt \times v, \tag{1}$$

where $dt = t_i - t_j$ and v is the trapped wave propagation velocity (1750 m.s^{-1}).

Given the 1 kHz sampling rate of the data, the depth estimates are discretized into 0.875 m intervals. The absolute uncertainty of the depth estimates, assuming a phase arrival time uncertainty of 3 ms and a propagation velocity uncertainty of 10%, is ~4 m. For about 10-15% of the events in each swarm, and primarily for small events with low signal-to-noise ratios, the automated picking algorithm generated erroneous arrival time estimates that could not be used for depth estimation, and these events were removed from the final catalog. We cannot estimate the seismic moment of the events because the amplitude of a trapped fluid mode is a function of radial position in the borehole, which is unknown for the hydrophones.

We estimated the average downward migration velocity of each swarm by using a weighted least squares method. Using the following fit equation: $\hat{d} = \beta_0 + \hat{v}t$ where $\hat{d}$ is the predicted depth, β_0 is the intercept, $\hat{v}$ is the estimated velocity reported in Figure 4, and t is the time of the event. The regression is weighted by the number of events in a 30-second window.

We estimated the instantaneous rupture front velocity during each swarm using a piecewise technique averaged over 10-second intervals. The process begins by selecting an initial event that represents the starting point of the migration. The algorithm then advances chronologically through the event catalog searching for the next event that is deeper than the initial event, and once a deeper event is encountered the instantaneous velocity for the period of time between those two events is calculated based on the differences in their depths and origin times. A threshold velocity, which was manually tuned to each swarm in the range 20-30 cm.s^{-1}, was used to prevent the algorithm from latching onto outliers. The deepest event becomes the initial event and the process is repeated until the end of the catalog is reached. The algorithm follows the leading edge of the rupture front and its piecewise nature allows it to follow the multiple strands observed during the day 188 swarm by starting at different times in the catalog. As a final step, time-averaged instantaneous velocity estimates are generated on 10-second intervals.

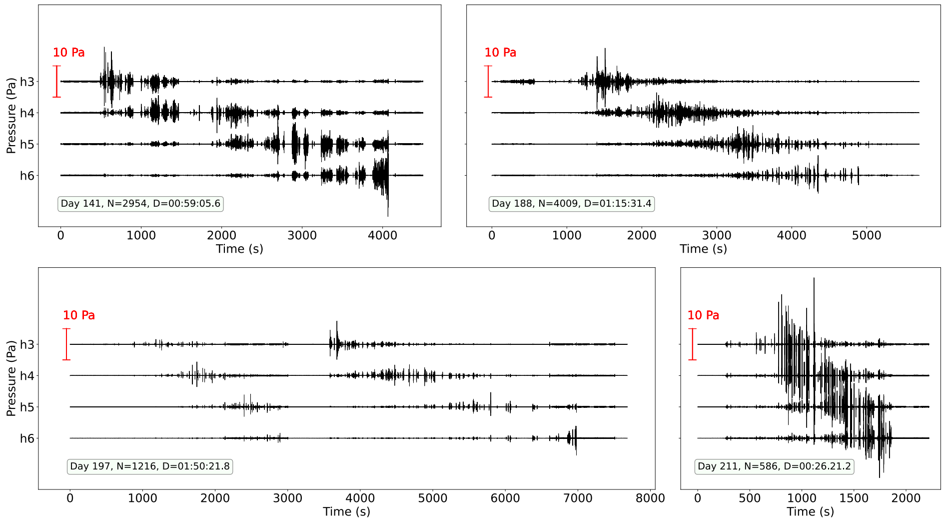

Figure 2. Raw hydrophone data for each event swarm, labeled by day of the year (2019). The number of detected events (N) and duration of the swarm (D) are reported in each panel.

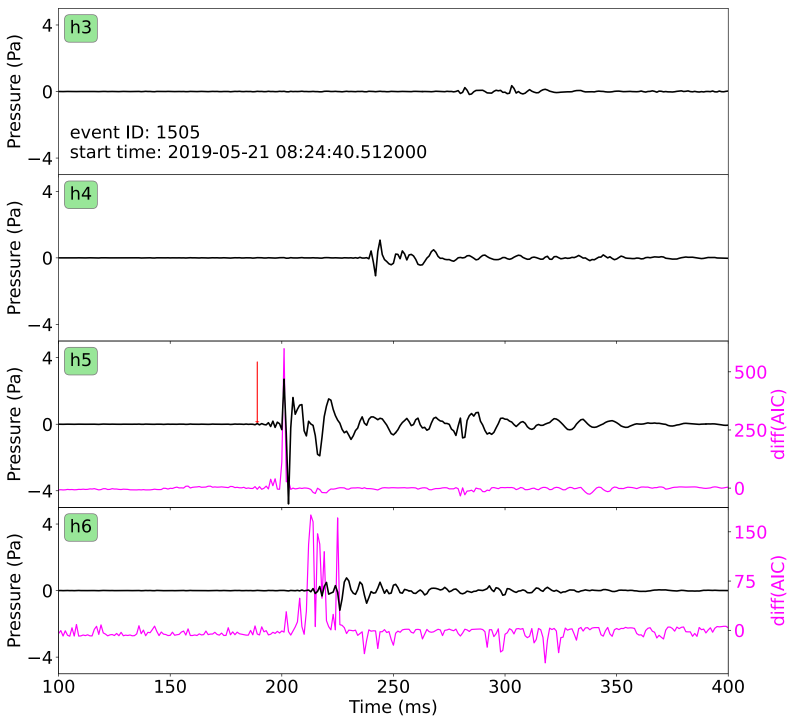

Figure 3. Example event detection with the AIC finite difference calculation which identifies the arrival times.

3 Results and Discussion

3.1 Detection of slow rupture swarms

Data records from borehole BA1A contain intense swarms of small, downward migrating rupture events that occurred during four days of the nine-month deployment (days 141, 188, 197, and 211 of the year 2019). The downward propagating nature of the events is evident in the raw vertical array data (Figure 2) and the impulsive events have typical acoustic amplitudes of $\leq$3 Pa, durations of $\sim$250 ms, and recurrence intervals of $<$ 1 s.

The individual swarms had event counts (N_x = count for swarm on day of year x) that varied from N_{141}=2954 to N_{188}=4009 to N_{197}=1216 to N_{211}=586, with durations (hour:minute:second) of D_{141}=00:59:06, D_{188}=01:16:31, D_{197}=01:50:22, and D_{211}=00:26:21. Each swarm began near the depth horizon of hydrophone h3 ($\sim$170 m) and migrated towards the bottom of the borehole (Figure 4). The migration patterns are patchy, with discrete depth intervals of fracturing interspersed with quiet zones where no events were detected. The swarms on days 141 and 211 exhibit an essentially monotonic downward migration but the swarms on days 188 and 197 are more complex (Figure 4). The swarm on day 188 appears to contain three distinct migration strands, indicating that multiple rupture fronts were active at the same time. The swarm on day 197 has two distinct migration episodes, with a weak, initial episode that did not reach the bottom of the borehole followed by a second, more energetic episode that reached the bottom of the hole.

We estimated the average downward migration rate of the events in each swarm and the instantaneous velocity of the migrating rupture front over the duration of each swarm as described in the Methods section. All of the swarms have median migration rates of $\sim$6-10 cm.s^{-1}, with the exception of the final swarm on day 211, which had the largest events and a faster average migration rate of $\sim$20 cm.s^{-1} (Figure 4). The instantaneous rupture front velocity estimates range from $\leq$ 1 cm.s^{-1} up to $\sim$15 cm s^{-1} for all swarms except that on day 211, which had a minimum velocity of 6 cm.s^{-1} and a maximum velocity of $\sim$30 cm.s^{-1}. There is no apparent correlation between depth and rupture front velocity and fracturing within a given depth interval continues at decreasing rates for $\sim$1 min after the front passes.

All of the rupture swarms observed in borehole BA1A occurred during a relatively short period of time when the borehole water levels were elevated following two large rain events (see Methods), with the first swarm occurring immediately after a sharp water level rise in May 2019 (Figure 5).

3.2 Rupture scenarios for the migrating swarms

Elastic stress variations are often at the origin of rupture in crustal rocks leading to either tensile or, more often, shear failure. In both cases, the propagating rupture rapidly accelerates toward the speed of the elastic waves (typically km/s (Scholz 2019)), which is substantially different from the slow migrations we observed over several hundreds of meters. All the swarms propagated at average rates of $\sim$6 to 20 cm.s^{-1}, similar to the propagation rate of slow-slip events observed in other fault systems (Sacks et al. 1978; Kaproth and Marone 2013; Ikari et al. 2013; Uchida et al. 2016; Gualandi et al. 2020; Ide and Beroza 2023). These rupture propagation velocities are often interpreted to be modulated by the combined effects of fluid transport and attendant variations in pore fluid pressure during slip (Segall et al. 2010; Brantut 2021; Ciardo and Lecampion 2019; Ozawa, Yang, and Dunham 2024). A rupture driven by change in fluid condition is then the most likely scenario, supported by the correlation between the onset of the swarms and high water levels in the borehole. A left-lateral strike-slip fault runs through the MBO site, but geological mapping and remote sensing imagery indicate that activity on this fault ceased $\sim$20 Ma (Callegari et al. 2022) and there is no evidence of activity in regional

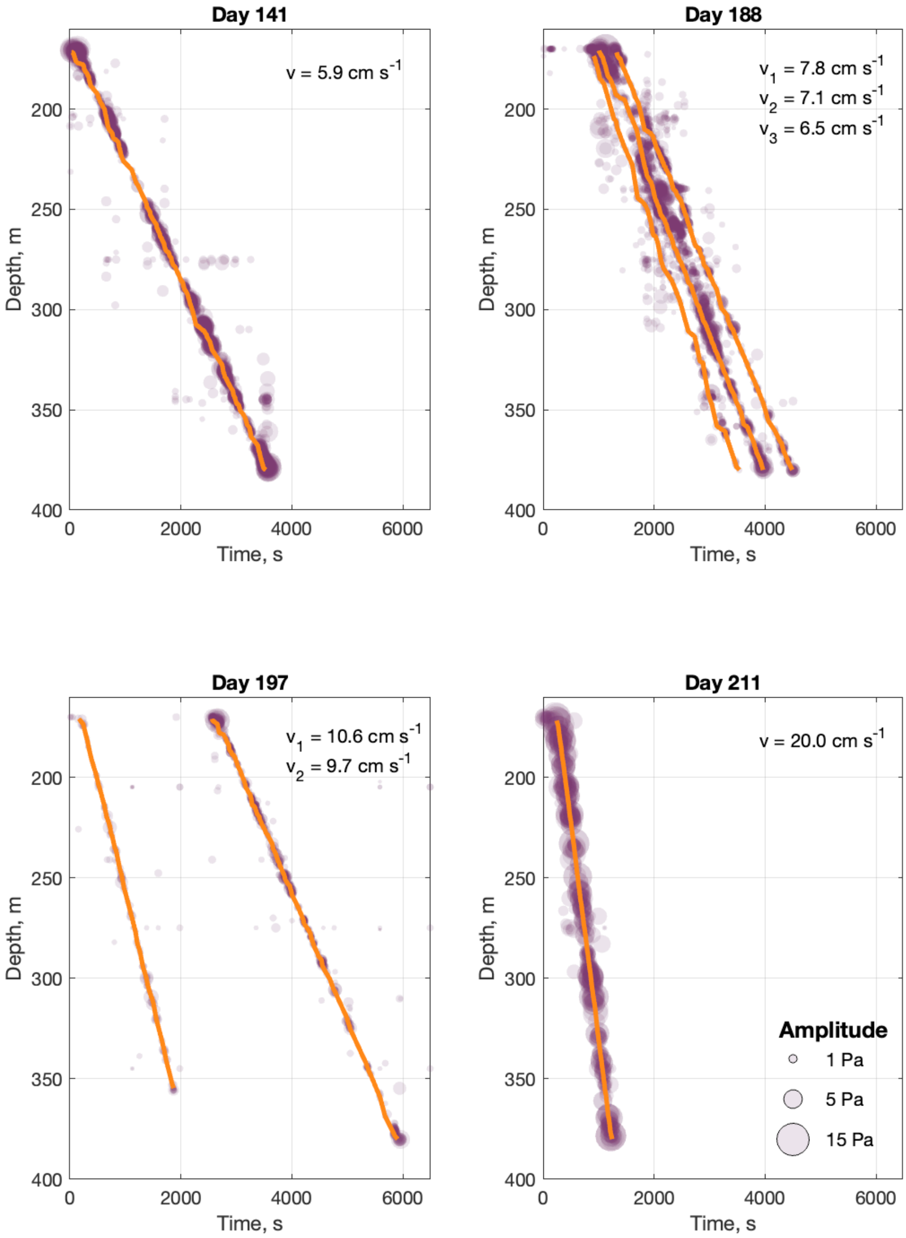

Figure 4. Event size and depth versus time for each swarm. Event size is shown by symbol size (see legend) and the solid orange lines indicate piecewise tracking of rupture fronts (see Methods). Median values of the instantaneous rupture front velocity estimates are listed.

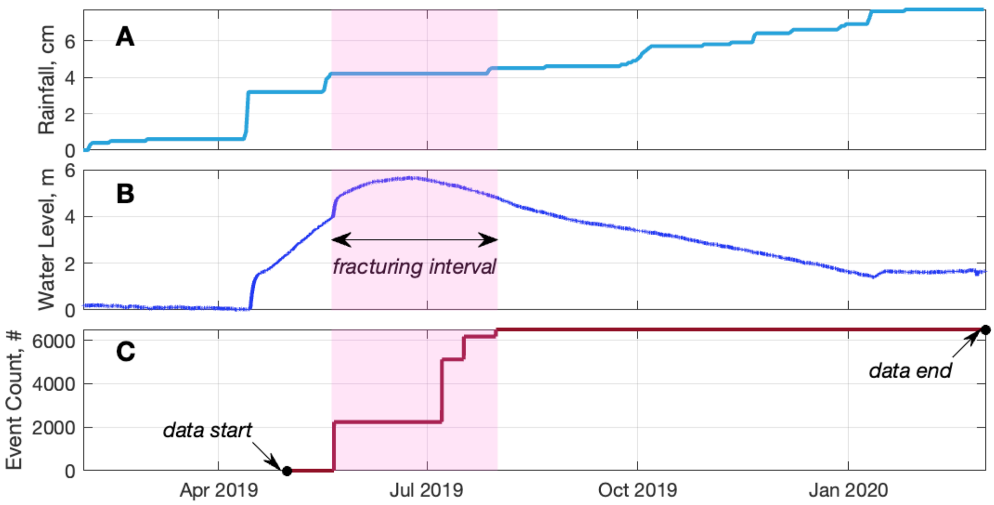

Figure 5. A) Cumulative daily precipitation for the MBO catchment. B) Relative water level data from borehole BA1D. C) Cumulative fracturing events count. The time interval during which the rupture swarms occurred is highlighted in the three panels.

earthquake catalogs or in our hydrophone array data. Additionally, most events observed in these seismic swarms have an amplitude of ≤ 3 Pa. Consequently, it seems very unlikely that the migrating swarms correspond to frictional slip activated by fluid pressure.

An increase of fluid pressure in the borehole can also cause tensile failure of the rock mass. At this depth, this is only possible in the direct vicinity of the borehole, which is consistent with the observed location of the swarm activities. The hoop stresses around a borehole are given by the Kirsch solution (Jaeger, N. G. Cook, and Zimmerman 2009):

$$\sigma_\theta = \frac{(\sigma_H + \sigma_h)}{2}(1 + \frac{a^2}{r^2}) - \frac{(\sigma_H - \sigma_h)}{2}(1 + 3\frac{a^4}{r^4})\cos 2\theta - P(\frac{a^2}{r^2}), \tag{2}$$

where a is the borehole radius, r is the radial distance from the borehole axis, θ is the angle from the maximum principal stress, P is the fluid pressure inside the borehole, and σ_H and σ_h are the local maximum and minimum principal stresses, respectively. Maximum tensile stresses are aligned with the maximum principal stress springline ($\theta \approx 0°$, $180°$), and if the length of a tensile crack growing away from the hole is much less than the borehole radius (i.e., $r \approx a$), the criterion for crack growth can be approximated by:

$$3\sigma_h - \sigma_H - p - \sigma_{wr} < -T. \tag{3}$$

In the equation above, T corresponds to the tensile strength of the rock and P has been decomposed as the sum of the fluid pressure p and the pressure caused by the growth of minerals from water rock reactions on the fracture surface σ_{wr}. Televiewer data from borehole BA1A reveals the presence of sub-vertical veins across the depth interval of the fracture swarms (Figure 6), and the depth interval of fracturing corresponds to the interval where the borehole fluid chemistry indicates active peridotite alteration (Kelemen, James A. Leong, et al. 2021). Taken together, these observations suggest a system that promotes tensile crack growth due to elevated pressure σ_{wr} caused by water-rock reactions on the freshly exposed crack surfaces. The volume increase due to mineralization

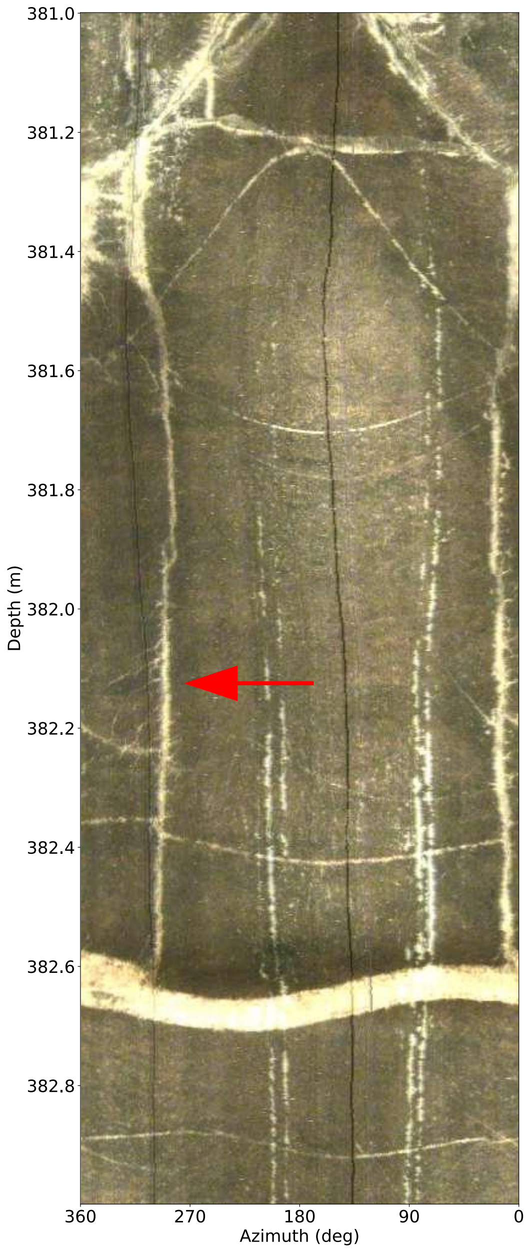

Figure 6. The borehole is transected by vertical white veins (example shown here). These veins are likely sites where active alteration could occur that allows for tensile fractures to nucleate and then propagate. The black line in the center of the image is a stitching artifact from the 360 degree televiewer image.

also maintains the fracture open and enables pore fluid circulation and pressurization, which is at the origin of the observed rupture swarms. As the tensile rupture is mainly driven by the increase in fluid pressure, its propagation is bounded by the speed at which pressurized fluid migrates into the fracture cavity. Using a hydraulic fracture model detailed in the appendix, we estimate that the downward migration speed should scale according to:

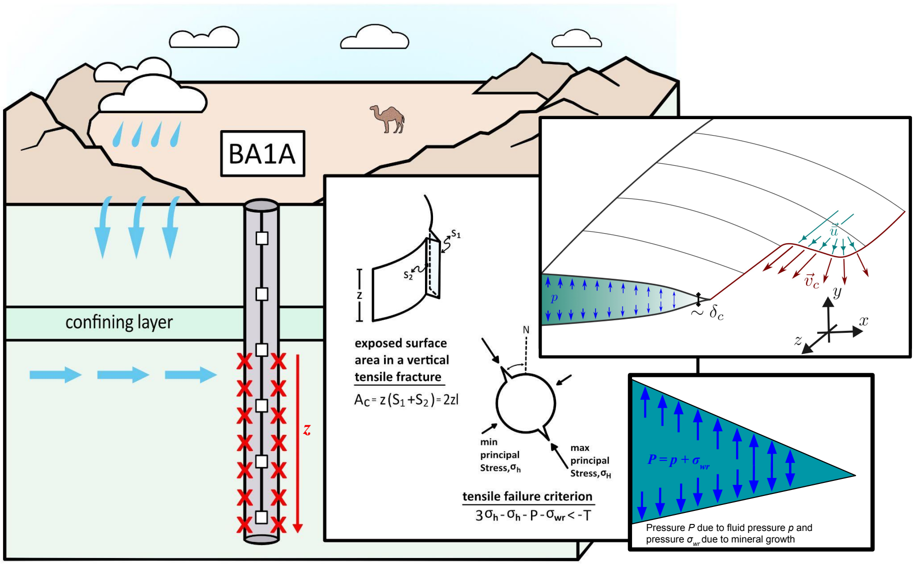

Figure 7. Boreholes BA1A and BA1D of the Oman Drilling Project Multi-Borehole Observatory. Drilling a borehole caused tensile fractures (inset, right) due to the relaxation of tectonic stresses. These fractures allowed fluid in the borehole (i.e., water) to infiltrate the fracture planes and over the two-year period this caused unaltered peridotites to serpentinize within the tensile fracture zone. Serpentinization of peridotite leads to a decrease in oxygen fugacity and increase in pH (Figure 1) as well a volumetric increase which causes strain (ϵ_s) on the surrounding rock. Rainfalls recharge the aquifer increasing the pore-pressure due to the confinement from the low porosity layer. This pore pressure increase reached a critical limit leading to downward migrating tensile fracture swarms in borehole BA1A.

$$v_{c,z} \sim \frac{\rho_w g}{\mu_w}\Big(\frac{K_{Ic}^2(1-\nu)}{\mathcal{G}T}\Big)^2. \quad (4)$$

In the equation above, μ_w and ρ_w characterize the pore fluid viscosity and density, $\mathcal{G}$, ν and $K_{I,c}$ describe the shear modulus, Poisson's ratio and tensile fracture toughness of the host rock, and g is the gravitational acceleration. Assuming nominal values of $K_{Ic} =$ 2MPa.m$^{1/2}$, $T = 5$ MPa, $\mathcal{G} = 20$ GPa, $\nu = 0.25$, $\rho_w = 1000$ kg.m^{-3}, and $\mu_w = 10^{-3}$ Pa.s yields a downward rupture speed on the order of a few cm.s^{-1}, in agreement with our observations. In addition, the model predicts that the rupture propagation speed should be independent of depth, which also agrees with our observations.

Tangential stresses decay rapidly with distance from the borehole. Typically, tensile fractures and breakouts only occur in the first hours to days after the creation of a borehole (Moore et al. 2011). Continued fracture growth more than two years after borehole BA1A was established requires a mechanism that maintains near-critical stress levels at the crack tips over time. The time-dependent parameters controlling tensile stress (Eq. 3) are fluid pressure, p, and water-rock reaction induced stresses, σ_{wr}, since the magnitude of the principal stresses, σ_H and σ_h, are unlikely to change on the timescale of our time series.

Given the short (~10 m) distance between boreholes BA1A and BA1D, and their similar hydrological structure (Lods et al. 2020), we can assume that the water level data from borehole BA1D provides a proxy for fluid pressure in borehole BA1A, and that it increased by ~54 kPa following large rain events in April and May, 2019. The correlation between the time interval of the fracture swarms and the interval of elevated fluid pressure demonstrates that fluid pressure could have played a role in triggering the swarms by lowering the effective stress. Fluid pressure changes of this magnitude are sufficient to trigger failure in critically stressed rock (e.g., (Ellsworth 2013)), and aquifer confinement may also play a role. All fracturing events observed in borehole BA1A were below the confining layer. Given that the increase in pore pressure is due to the aquifer being recharged by rain, this implies that recharge from the surrounding mountains occurs at a depth below the local confining layer at ~100 m.

3.3 Reaction-induced fracturing and estimates of mineralization rates

All of the fracturing events we observed occur within the depth interval (150-400 m) where the pH and oxygen fugacity of the borehole fluids indicates active peridotite alteration (Figure 1, (Kelemen, James A. Leong, et al. 2021)). Repeated, reaction-driven opening and propagation of a pre-existing fracture may occur when fluid-rock reaction products partially fill the fracture aperture, and exert a crystallization pressure on the fracture walls. This suggests that water-rock interactions may play a role in maintaining crack tip stress at near-critical levels. Here we discuss the reactions involved that lead to these volumetric expansions that create stress to maintain the rock wall of the BA1A borehole at critical levels.

Peridotite alteration can lead to a 40-60% volume increase depending on the fraction of Fe^{2+} contained in the olivine (Jamtveit, Putnis, and Malthe-Sørenssen 2009; Kelemen, Juerg Matter, et al. 2011), and we can propose order of magnitude estimates for the rate at which fractures in the peridotite surrounding the OmanDP boreholes might fill with reaction products as follows. Using simplified, iron-free mineral stoichiometry, the reaction between water and olivine to form serpentine and carbonate is given by:

$$2\,Mg_2SiO_4 + CO_2 + 2\,H_2O \longrightarrow Mg_3Si_2O_5(OH)_4 + MgCO_3. \quad (5)$$

This reaction increases the solid volume by 67%, and may be rate-limited by olivine dissolution at low temperature, producing e.g., 5E-10 moles olivine m^{-2}.s^{-1} at a temperature of 40°C and pH 8 to 10 (rates at 25°C are from (Oelkers et al. 2018), borehole fluid pH and temperature are from (Kelemen, James A. Leong, et al. 2021)), corresponding to 0.015 moles m^{-2}.year^{-1}. If we assume that olivine within 0.3 mm of the fracture walls participates in this reaction, then, given an olivine density of 3300 kg.m^{-3}, ∼2 g or 0.014 moles Mg-olivine per m^2 of surface area along the crack walls will dissolve in about a year, consuming 6 mm of olivine and producing 10 mm of reaction products. The crystallization pressure generated by this reaction depends on the crack aperture, and given the estimates from Eq. 5 based on critical opening distance (∼0.1 to 1 mm), the reaction products will fill most or all of the pore space and can thus generate significant crystallization pressures on annual timescales.

In reality, the crack walls are composed of both olivine and serpentinite (about 85 vol% serpentine + 15 vol% brucite) produced by olivine hydration, for example by the following simplified reactions:

$$2\,\mathsf{Mg_2SiO_4} + 3\,\mathsf{H_2O} \longrightarrow \mathsf{Mg_3Si_2O_5(OH)_4} + \mathsf{Mg(OH)_2}, \tag{6}$$

$$\mathsf{Fe^{II}{}_2SiO_4} + \mathsf{Mg_2SiO_4} + 3\,\mathsf{H_2O} \longrightarrow \mathsf{Fe^{II}{}_2MgSi_2O_5(OH)_4} + \mathsf{Mg(OH)_2}. \tag{7}$$

Continued carbonation of Mg-serpentine (e.g., $\mathsf{serpentine} + \mathsf{CO_2} \longrightarrow \mathsf{talc} + \mathsf{H_2O}$) is not likely occurring at the low $\mathsf{CO_2}$ fugacities of the borehole fluids, and talc is rare or absent in drill core. Brucite carbonation reactions and combined iron oxidation and carbon mineralization reactions, however, are both ongoing in the rocks surrounding the boreholes (Kelemen, James A. Leong, et al. 2021). We can thus consider two more simplified reactions:

$$\mathsf{Mg(OH)_2} + \mathsf{CO_2} \longrightarrow \mathsf{MgCO_3} + \mathsf{H_2O}, \tag{8}$$

with a solid volume increase of 95%, and

$$\mathsf{Fe^{II}{}_2MgSi_2O_5(OH)_4} + \mathsf{CO_2} + \mathsf{H_2O} \longrightarrow \mathsf{Fe^{III}{}_2Si_2O_5(OH)_4} + \mathsf{MgCO_3} + \mathsf{H_2}, \tag{9}$$

with a solid volume increase of 38%. The rates of these reactions are less well constrained, but (James Andrew Leong et al. 2023) showed that Fe oxidation and $\mathsf{H_2}$ production rates measured in Oman serpentinites are consistent, within an order of magnitude, with the olivine dissolution rate data (Oelkers et al. 2018). Thus, given the uncertainties involved, these combined reactions yield a similar result to the simpler olivine weathering reaction 5. These calculations suggest that the changes in pH and oxygen fugacity measured in the BA1A fluids are caused by fluid-rock interactions that produce hydrogen (and increase pH) and reduce oxygen fugacity, and consequently increase stresses on the wall of borehole BA1A.

4 Conclusion

Our results demonstrate that sub-vertical tensile cracks continued to grow into the actively serpentinizing peridotite rocks surrounding borehole BA1A of the OmanDP MBO more than two years after the hole was established. The chemically weakened rock fractured when pore pressure in the semi-confined portion of the local aquifer increased following large rain events. This indicates that crack tip stresses remained at near-critical levels such that fracture growth could be stimulated with a modest (∼50 kPa) increase in pore pressure, suggesting that it may not be difficult to stimulate fracture growth for geological carbon sequestration efforts planned for the MBO site, or other sites like it. Indeed, it is possible to consider that there could be a climatic impact on the carbon absorption at ophiolite outcrops. Rains in places where confining aquifers allow for pore pressure increases would increase the likelihood of fluid filled peridotite cracks to fracture and promote fluid to access unaltered rock. In places where this could occur it may be that the reaction-driven hypothesis needs an additional component, the climate. As rain would regularly increase pore pressure in confining wells, they would regularly accelerate the stress accumulation at reaction-driven cracking tips. This paints a complex picture and will require further study at other ophiolite outcrop sites in order to fully understand the climatic impact on the reaction-driven fracturing hypothesis.

Our analysis indicates that the fracture propagation rates were limited by the ability of pore fluids to flow into newly opened pore volume at the fracture tips, which is a strikingly similar process to the dilatant hardening mechanism often invoked to explain shear rupture during slow earthquakes in crustal regions with high fluid pressure (Sacks et al. 1978; Kaproth and Marone 2013; Ikari et al. 2013).

Appendix A: Hydraulic fracture problem

The hydraulic fracture setup is sketched in Figure 7 of the main text.

In situ-stress conditions

As discussed in the main text, the tensile fracture is caused by the elastic stress perturbation due to the borehole, such that the tensile traction along the crack face can be written as

$$\tau_n(x, z) = \sigma_H(z) + p(x, z) - 3\sigma_h(z) + \sigma_{wr}, \tag{10}$$

where σ_H and σ_h are respectively the largest and lowest compressive stress and σ_{wr} accounts for the increase in normal stress due to chemical alteration of the rock. The borehole stress conditions and active mineralization ensure that fracture remains open despite the confining stress at depth.

Boundary and initial conditions

Fluid pressure is assumed to be hydrostatic within the fracture between swarms $p(x, z) = \rho_w g z$. A rupture event initiates at the depth of the confining layer due to a local increase in fluid pressure.

Fluid flow

During swarms, the crack grows and fluid invades the newly created fracture cavity. Following hydraulic fracture, we assume a Poiseuille fluid velocity profile such that flow is characterized by an average flow rate $\vec{\bar{u}}$ across the thin aperture δ. Neglecting the contribution of inertia and fluid exchange with the host rock, lubrication flow through the fracture can be expressed as a two-components vector:

$$\vec{\bar{u}} = -\frac{\delta^2}{12\mu_w}(\nabla p - \rho_w \vec{g}). \tag{11}$$

In the radial direction r, flow rate is driven by the gradient in pressure created by the motion of the fracture tip and the associated fluid pressure drops. During crack growth, hydraulic fracture model and experiments typically observe a transient lag between the fronts of the invading fluid and the one of the propagating crack tip, such that fluid pressure is assumed to be vanishingly small in the near-tip region $r = a$.

In the vertical direction h, fluid is flowing downwards driven by vertical pressure gradient plus a gravitational contribution.

Fracture mechanics

Crack growth is assumed to follow the description of Linear Elastic Fracture Mechanics and arises as long as the tensile stress intensity factor at the tip exceeds the fracture toughness of the rock $K_{I,c}$. Due to the large confining stresses existing far from the borehole, the radial expansion of the crack during each event is expected to be small compared to the initial crack size, which is supported by the small amplitudes of the measured acoustic events. From the observed dynamics of the swarms, crack growth starts from the confining layer and progressively migrates downwards. Interestingly, a similar tangential crack growth is also observed at the laboratory scale in the context of fluid-driven fracture (Cochard et al. 2024). From hydraulic fracture theory, crack propagation speed is quasi-static and well approximated by the velocity of lubrication flow in the near-tip region $\vec{v}_c \approx \vec{\bar{u}}(r = a)$.

As sketched in Figure 7, the vertical flow in the freshly created fracture space is of particular interest and arises through the low-pressure, small-aperture region near the tip. Invoking these conditions, we assume that, in the near-tip cavity, the gravity term in Eq.(11) dominates the pressure gradient along the vertical direction. This assumption is further supported by the fact that crack growth arises over much larger distances along the vertical direction than along the radial direction. The vertical crack propagation speed can then be written as:

$$v_{c,z} = \frac{\delta^2}{12\mu}\rho g. \tag{12}$$

Last, we use a cohesive zone model of fracture to estimate the order of magnitude of the crack aperture in the tip region from the critical opening distance $\delta(r = a, z)/\delta_c \approx 1 - 10$. The latter is expressed as function of the fracture toughness $K_{I,c}$, the tensile strength T and the elastic parameters of the host rock:

$$\delta_c = \alpha\frac{K_{I,c}^2(1-\nu)}{\mathcal{G}T}, \tag{13}$$

with $\mathcal{G}$ and ν being respectively the shear modulus and Poisson's ratio of the host rock and α a constant that corresponds to unity for linear cohesive law or to $\alpha = e$ for exponential cohesive law. The combination of Eqs. (12) and (13) leads to the scaling of the swarm migration speed reported in Eq. (4) of the manuscript.

Open Research Section

Hydrophone data have been archived at the IRIS DMC (network code 7F 2019-2020, `https://doi.org/10.7914/SN/7F_2019`). The lithological data, borehole BA1D water level data, and televiewer data can be downloaded from the Inter-Continental Drilling Program data repository `https://www.icdp-online.org/projects/by-continent/asia/oodp-oman/public-data-1`. Precipitation data is available through the Copernicus data repository and Google Earth Engine `https://code.earthengine.google.com/65cfcd01ee34290615a7c854a00b76f4`. Please see supplemental python and matlab codes in the associated github repository: `https://github.com/SerpRateAI/tensilePaper`.

Acknowledgments

This project received funding from the Norwegian Research Council (SerpRateAI, grant no. 334395), the European Research Council under the ERC Advanced Grant no. 101019628 "Break Through Rocks", and the US National Science Foundation (grant no. EAR-1516313). We thank Paul Fucile for his efforts to design and install the hydrophone arrays. John M. Aiken also would like to thank Varvara Bazilova who taught how to analyse ERA5-land and HydroBASINS data sets using Google Earth Engine and which was invaluable to this work. François Renard and Fabian Barras acknowledge support from the project FricFrac funded by the Center for Advanced Study (CAS) at the Norwegian Academy of Science and Letters during the academic year 2023-2024. The authors are grateful to Issa El-Hussain and Sultan Qaboos University for logistical assistance with the fieldwork. The authors thank the Ministry of Regional Municipalities and Water Resources in the Sultanate of Oman (particularly Eng. Sadi Al Habsi, Dr. Rashid Al Abri, Eng. Haider Ahmed Mohammed Alajmi, Ali Al Shukali Eng. Abduallah Al Kasbi, Said Al Mangi), and Eng. Zaher Al Sulaimani and Mazin Al Sulaimani from AZD Engineering for their logistical and technical support.

References

Gislason, Sigurdur R and Eric H. Oelkers (2014). "Carbon storage in basalt". In: *Science* 344.6182, pp. 373–374.

Iyer, Kyle. et al. (2008). "Reaction-assisted hierarchical fracturing during serpentinization". In: *Earth and Planetary Science Letters* 267.3, pp. 503–516. ISSN: 0012-821X. DOI: https://doi.org/10.1016/j.epsl.2007.11.060.

Kelemen, Peter B., James A. Leong, et al. (2021). "Initial Results From the Oman Drilling Project Multi-Borehole Observatory: Petrogenesis and Ongoing Alteration of Mantle Peridotite in the Weathering Horizon". In: *Journal of Geophysical Research: Solid Earth* 126.12, e2021JB022729. DOI: https://doi.org/10.1029/2021JB022729.

Aiken, John M et al. (2024). "A framework for an AI pipeline for borehole data". In: *Authorea Preprints*.

Kelemen, Peter B. and Jürg Matter (2008). "In situ carbonation of peridotite for CO¡sub¿2¡/sub¿ storage". In: *Proceedings of the National Academy of Sciences* 105.45, pp. 17295–17300. DOI: 10.1073/pnas.0805794105.

Jamtveit, Bjørn, Christine V Putnis, and Anders Malthe-Sørenssen (2009). "Reaction induced fracturing during replacement processes". In: *Contributions to Mineralogy and Petrology* 157.1, pp. 127–133. DOI: 10.1007/s00410-008-0324-y.

Renard, François (2021). "Reaction-induced fracturing: When chemistry breaks rocks". In: *Journal of Geophysical Research: Solid Earth* 126.2, e2020JB021451.

Templeton, Alexis S. et al. (2021). "Accessing the Subsurface Biosphere Within Rocks Undergoing Active Low-Temperature Serpentinization in the Samail Ophiolite (Oman Drilling Project)". In: *Journal of Geophysical Research: Biogeosciences* 126.10. e2021JG006315 2021JG006315, e2021JG006315. DOI: https://doi.org/10.1029/2021JG006315.

Hatakeyama, Kohei et al. (2021). "Effects of Alteration and Cracks on the Seismic Velocity Structure of Oceanic Lithosphere Inferred From Ultrasonic Measurements of Mafic and Ultramafic Samples Collected by the Oman Drilling Project". In: *Journal of Geophysical Research: Solid Earth* 126.11, e2021JB021923. DOI: https://doi.org/10.1029/2021JB021923.

Callegari, Ivan et al. (2022). "Tectonic transition from thrusting to polyphase non-confining deformation within the Semail Ophiolite along the sinistral, transtensional Issmaiya Fault Zone (Sultanate of Oman)". In: *Journal of Asian Earth Sciences* 224, p. 105007. ISSN: 1367-9120. DOI: https://doi.org/10.1016/j.jseaes.2021.105007.

Sohn, R.A. and J.M. Matter (2023). "The response of borehole water levels in an ophiolitic, peridotite aquifer to atmospheric, solid Earth, and ocean tides". In: *Journal of Hydrology X* 21, p. 100163. ISSN: 2589-9155. DOI: https://doi.org/10.1016/j.hydroa.2023.100163.

Jaeger, John Conrad, Neville GW Cook, and Robert Zimmerman (2009). *Fundamentals of rock mechanics*. John Wiley & Sons. DOI: 10.1017/CBO9780511735349.

Zoback, Mark D. et al. (1985). "Well bore breakouts and in situ stress". In: *Journal of Geophysical Research: Solid Earth* 90.B7, pp. 5523–5530. DOI: https://doi.org/10.1029/JB090iB07p05523.

Zheng, Ziqiong, John Kemeny, and Neville G. W. Cook (1989). "Analysis of borehole breakouts". In: *Journal of Geophysical Research: Solid Earth* 94.B6, pp. 7171–7182. DOI: https://doi.org/10.1029/JB094iB06p07171.

Kelemen, Peter B., Juerg Matter, et al. (2011). "Rates and Mechanisms of Mineral Carbonation in Peridotite: Natural Processes and Recipes for Enhanced, in situ CO2 Capture and Storage". In: *Annual Review of Earth and Planetary Sciences* 39.1, pp. 545–576. DOI: 10.1146/annurev-earth-092010-152509.

Moore, J. Casey et al. (2011). "Growth of borehole breakouts with time after drilling: Implications for state of stress, NanTroSEIZE transect, SW Japan". In: *Geochemistry, Geophysics, Geosystems* 12.4. DOI: https://doi.org/10.1029/2010GC003417.

Lods, Gérard et al. (2020). "Groundwater flow characterization of an ophiolitic hard-rock aquifer from cross-borehole multi-level hydraulic experiments". In: *Journal of Hydrology* 589, p. 125152. ISSN: 0022-1694. DOI: https://doi.org/10.1016/j.jhydrol.2020.125152.

Kelemen, Peter B., J.M. Matter, et al. (2020). "Scientific Drilling in the Samail Ophiolite, Sultanate of Oman". In: *Proceedings of the Oman Drilling Project*. DOI: 10.14379/Oman.ph1-2.proc.2020.

Katayama, Ikuo et al. (2020). "Permeability Profiles Across the Crust-Mantle Sections in the Oman Drilling Project Inferred From Dry and Wet Resistivity Data". In: *Journal of Geophysical Research: Solid Earth* 125.8, e2019JB018698. DOI: https://doi.org/10.1029/2019JB018698.

(CDS), Copernicus Climate Change Service Climate Data Store (2017). *Copernicus Climate Change Service (C3S) (2017): ERA5: Fifth generation of ECMWF atmospheric reanalyses of the global climate*. Accessed 2024-01-25. DOI: 10.1002/qj.3803. URL: https://cds.climate.copernicus.eu/cdsapp#!/home.

Lehner, Bernhard and Günther Grill (2013). "Global river hydrography and network routing: baseline data and new approaches to study the world's large river systems". In: *Hydrological Processes* 27.15, pp. 2171–2186. DOI: https://doi.org/10.1002/hyp.9740.

Maeda, Naoki (1985). "A method for reading and checking phase times in autoprocessing system of seismic wave data". In: *Zisin* 38, pp. 365–379. DOI: https://doi.org/10.4294/zisin1948.38.3_365.

Schoenberg, Michael et al. (Nov. 1981). "Space–time dependence of acoustic waves in a borehole". In: *The Journal of the Acoustical Society of America* 70.5, pp. 1496–1507. ISSN: 0001-4966. DOI: 10.1121/1.387107.

Scholz, Christopher H (2019). *The mechanics of earthquakes and faulting*. Cambridge university press.

Sacks, I Selwyn et al. (1978). "Slow earthquakes and stress redistribution". In: *Nature* 275.5681, pp. 599–602. DOI: https://doi.org/10.1038/275599a0.

Kaproth, Bryan M. and C. Marone (2013). "Slow Earthquakes, Preseismic Velocity Changes, and the Origin of Slow Frictional Stick-Slip". In: *Science* 341.6151, pp. 1229–1232. DOI: 10.1126/science.1239577.

Ikari, Matt J et al. (2013). "Slip weakening as a mechanism for slow earthquakes". In: *Nature geoscience* 6.6, pp. 468–472. DOI: https://doi.org/10.1038/ngeo1818.

Uchida, Naoki et al. (2016). "Periodic slow slip triggers megathrust zone earthquakes in northeastern Japan". In: *Science* 351.6272, pp. 488–492. DOI: 10.1126/science.aad3108.

Gualandi, A. et al. (2020). "The predictable chaos of slow earthquakes". In: *Science Advances* 6.27, eaaz5548. DOI: 10.1126/sciadv.aaz5548.

Ide, Satoshi and Gregory C Beroza (2023). "Slow earthquake scaling reconsidered as a boundary between distinct modes of rupture propagation". In: *Proceedings of the National Academy of Sciences* 120.32, e2222102120. DOI: https://doi.org/10.1073/pnas.2222102120.

Segall, Paul et al. (2010). "Dilatant strengthening as a mechanism for slow slip events". In: *Journal of Geophysical Research: Solid Earth* 115.B12. DOI: https://doi.org/10.1029/2010JB007449.

Brantut, Nicolas (Nov. 2021). "Dilatancy Toughening of Shear Cracks and Implications for Slow Rupture Propagation". In: *Journal of Geophysical Research: Solid Earth* 126.11. ISSN: 2169-9313, 2169-9356. DOI: 10.1029/2021JB022239.

Ciardo, F. and B. Lecampion (2019). "Effect of Dilatancy on the Transition From Aseismic to Seismic Slip Due to Fluid Injection in a Fault". In: *Journal of Geophysical Research: Solid Earth* 124.4, pp. 3724–3743. DOI: https://doi.org/10.1029/2018JB016636.

Ozawa, So, Yuyun Yang, and Eric M. Dunham (2024). "Fault-Valve Instability: A Mechanism for Slow Slip Events". In: *Journal of Geophysical Research: Solid Earth* 129.10, e2024JB029165. DOI: https://doi.org/10.1029/2024JB029165.

Ellsworth, William L. (2013). "Injection-Induced Earthquakes". In: *Science* 341.6142, p. 1225942. DOI: 10.1126/science.1225942.

Oelkers, Eric H. et al. (2018). "Olivine dissolution rates: A critical review". In: *Chemical Geology* 500, pp. 1–19. ISSN: 0009-2541. DOI: https://doi.org/10.1016/j.chemgeo.2018.10.008.

Leong, James Andrew et al. (2023). "H2 and CH4 outgassing rates in the Samail ophiolite, Oman: Implications for low-temperature, continental serpentinization rates". In: *Geochimica et Cosmochimica Acta* 347, pp. 1–15. ISSN: 0016-7037. DOI: https://doi.org/10.1016/j.gca.2023.02.008.

Cochard, T. et al. (2024). "Propagation of extended fractures by local nucleation and rapid transverse expansion of crack-front distortion". In: *Nature Physics* 20, pp. 660–665. DOI: https://doi.org/10.1038/s41567-023-02365-0.